Combined effects of compressibility and slip in flows of a Herschel–Bulkley fluid

Yiolanda Damianou [a], Georgios C. Georgiou [a,*], Irene Moulitsas [b]

[a] Department of Mathematics and Statistics, University of Cyprus, P.O. Box 20537, 1678 Nicosia, Cyprus
[b] The Cyprus Institute, 17 Kypranoros Street, 1061 Nicosia, Cyprus

ARTICLE INFO

ABSTRACT

In this work, the combined effects of compressibility and slip in Poiseuille flows of Herschel–Bulkley fluids are investigated. The density is assumed to obey a linear equation of state, and wall slip is assumed to follow Navier's slip condition with zero slip yield stress. The flow is considered to be weakly compressible so that the transverse velocity component is zero and the pressure is a function of the axial coordinate. Approximate semi-analytical solutions of the steady, creeping, plane and axisymmetric Poiseuille flows are derived and the effects of compressibility, slip, and the Bingham number are discussed. In the case of incompressible flow, it is shown that the velocity may become plug at a finite critical value of the slip parameter which is inversely proportional to the yield stress. In compressible flow with slip, the velocity tends to become plug upstream, which justifies the use of one-dimensional models for viscoplastic flows in long tubes. The case of pressure-dependent slip is also investigated and discussed.

1. Introduction

Slip at the wall occurs in many flows of complex fluids, such as suspensions, emulsions, polymer melts and solutions, miscellar solutions, and foams, leading to very interesting phenomena and instabilities. The implications of slip have been reviewed by various researchers [1,2]. In order to better understand and simulate slip effects, it is necessary to have realistic slip velocity models. In a recent review, Hatzikiriakos [2] classified slip models into static (weak slip) and dynamic ones and pointed out that the former are not valid in transient flows, since slip relaxation effects might become important, leading to delayed slip and other phenomena.

The experimental data show that the slip velocity is in general a function of the wall shear stress, the wall normal stress (which includes pressure), the temperature, the molecular weight and its distribution, and the fluid/wall interface, e.g. the interaction between the fluid and the solid surface and surface roughness (see Ref. [1] and references therein). Neto et al. [3] reviewed experimental studies of wall slip of Newtonian liquids and discussed the effects of surface roughness, wettability, and the presence of gaseous layers. More recently, Sochi [4] reviewed slip at fluid–solid interfaces from different perspectives, such as slip factors, mechanisms, and measurement, and discussed, in particular, slip with non-Newtonian behavior, i.e. yield stress, viscoelasticity, and time dependency.

In the present work we focus on the effects of wall shear stress and pressure on the steady-state slip velocity. Therefore, we discuss only static slip models and refer the reader to the review of

Hatzikiriakos [2] for dynamic slip models. Navier [5] was the first to propose a slip model relating linearly the slip velocity u_w, i.e. the fluid velocity relative to the adjacent wall, to the wall shear stress, τ_w:

$$u_w = \alpha \tau_w \tag{1}$$

α being the slip coefficient. The slip coefficient varies in general with temperature, normal stress, and pressure, molecular parameters, and the characteristics of the fluid/wall interface. Obviously, for $\alpha = 0$, we have no slip, while for $\alpha \rightarrow \infty$ we get perfect slip. The slip coefficient is also defined by

$$\alpha \equiv \frac{b}{\eta} \tag{2}$$

where η is the viscosity and b is the extrapolation length, i.e. the characteristic length equal to the distance that the velocity profile at the wall must be extrapolated to reach zero. More complex, non-linear slip equations have also been proposed. A power-law expression,

$$u_w = \alpha \tau_w^m \tag{3}$$

where m is the power-law exponent, has been widely employed by several investigators (see, e.g., [6,7]).

Experimental data on several fluid systems, such as linear polymers (mainly polyethylenes) [8,9], highly entangled polymers [10], pastes [11], and colloidal suspensions [12], indicate that slip occurs only when the stress exceeds a critical value τ_c, which is similar to a Coulomb friction term and can be viewed as a "wall shear", or "interfacial", or, simply, "slip" yield stress. Hatzikiriakos and Dealy [9] pointed out that slip model (3) fails to describe the slip velocity

* Corresponding author. Tel.: +357 22892612; fax: +357 22892601.
E-mail address: georgios@ucy.ac.cy (G.C. Georgiou).

in the neighborhood of τ_c, which is critical in understanding polymer slip phenomena. They thus used the following Bingham-type equation:

$$u_w = \begin{cases} 0, & \tau_w \leqslant \tau_c \\ \alpha \tau_w^m, & \tau_w \geqslant \tau_c \end{cases} \tag{4}$$

The following general phenomenological slip equation

$$u_w = \begin{cases} 0, & \tau_w \leqslant \tau_c \\ \alpha(\tau_w - \tau_c)^m, & \tau_w \geqslant \tau_c \end{cases} \tag{5}$$

has been used by various researchers in the analysis of squeeze flow of generalized Newtonian fluids with apparent wall slip [13,14].

As already mentioned, the dependence of the slip velocity on the normal stress is weaker than that on the shear stress. In general, slip velocity decreases with pressure, i.e. slip occurs near the exit of a tube and is reduced upstream. Experimental evidence for this phenomenon was provided in the late sixties by Vinogradov and Ivanova [15] who carried out capillary extrusion experiments showing that melt fracture was suppressed at elevated pressures, an effect attributed to the reduction of slip at high pressures. Hill et al. [6] proposed a framework of adhesive failure between a highly-stressed polymer melt and the wall based on the theory of elastomer adhesion, which leads to a slip relation for polyethylene melts that shows a power-law dependence of the slip velocity on the wall shear stress and an exponential dependence on the isotropic pressure:

$$u_w = \alpha_1 e^{-\alpha_2 p} \tau_w^m \tag{6}$$

where α_1 and α_2 are material constants and p is the pressure. The same expression was later used by Person and Denn [16] in a study of the flow of a power-law fluid in a channel. Similarly, Hatzikiriakos and Dealy [7] formulated a theoretical model based on an extension of analysis of Lau and Schowalter [17], whose form is similar to that of Eq. (8), despite its different theoretical basis. However, they found a stronger pressure dependence at moderate pressures and saturation at higher pressures [7].

Tang and Kalyon [18] developed a mathematical model describing the time-dependent pressure-driven flow of compressible polymeric liquids subject to pressure-dependent slip and reported that undamped periodic oscillations in pressure and mean velocity are observed when the boundary condition changes from weak to strong slip. In order to describe the pressure dependence of the slip coefficient, they used the following expression

$$\alpha = \alpha_1 \left(\frac{p_0}{p}\right)^\kappa \tag{7}$$

where p is the atmospheric pressure. The positive exponent κ is equal to 1 for Knudsen flow (i.e. for compressible gas flow) and is determined experimentally for polymer melts and suspensions.

With the exception of some recent applications in micro- and nano-fluidics, the issue of wall slip for Newtonian fluids has been of rather limited interest [1]. The present work concerns fluid systems with a yield stress, such as concentrated suspensions, gels, foams, drilling fluids, food products, and nanocomposites, for which wall slip is commonplace [4] and may lead to spectacular effects [13]. In the case of concentrated suspensions, slip is due to the displacement of the disperse phase away from solid walls [19]. Sochi [4] points out that slip effects in non-Newtonian systems become particularly important, since they affect the shear rate near the wall and thus shear-rate-dependent parameters, such as the viscosity. In their review paper on squeeze flow theory, Engmann et al. [20] considered a wide class of materials, including yield-stress and viscoelastic fluids, and pointed out that reliable results can be obtained only if wall slip effects are taken into account.

There are numerous experimental works demonstrating slip with viscoplastic materials. The hydraulic fracturing gels studied by Jiang et al. [21] obeyed a Herschel–Bulkley constitutive equation and followed a power-law slip equation. Yilmazer and Kalyon [13] studied slip effects in capillary and parallel disk torsional flows of highly filled suspensions and found that the slip velocity increased approximately linearly with the shear stress (at high values of the wall shear stress). Moreover, they reported that, due to wall slip, the velocity in capillary flows is almost plug above a critical shear stress. Piau [22] studied the rheology and slip of carbopol gels in rheometers. He used the Herschel–Bulkley constitutive equation to describe their rheology and slip Eq. (5) (with $m = 1$) to describe slip at the wall. Foams are also known to exhibit both yield stress and slip [23,24]. Ballesta et al. [12] employed a linear slip equation with a threshold shear stress (Eq. (5)) for hard-sphere colloidal glasses obeying the Herschel–Bulkley constitutive equation. Ardakani et al. [25] performed experiments on a commercial toothpaste and showed the existence of yield stress and thixotropy. They also reported that severe slip occurs in capillary flow with different die designs and employed a linear relationship for slip, in order to simulate toothpaste extrusion.

Many important applications require the study of weakly compressible flows of yield-stress fluids. A notable example is the time-dependent flow of waxy crude oils in a tube investigated numerically by Vinay et al. [26], who employed the Bingham model and an exponential equation of state and used the augmented Lagrangian method. Belblidia et al. [27] solved the time-dependent, weakly compressible extrudate-swell flow of a Herschel–Bulkley fluid. Their study showed that extrudate swell is unaltered by compressibility under no-slip wall conditions. They pointed out that "it is expected that this position will be altered under slip-wall settings". Taliadorou et al. [28] derived approximate semi-analytical solutions of the axisymmetric and plane Poiseuille flows of weakly compressible Herschel–Bulkley fluid with no slip at the wall. The two-dimensional axial velocity was assumed to be given by an expression similar to that for the incompressible flow, with the pressure-gradient and the yield stress point assumed to be functions of the axial coordinate. The effects of compressibility have been studied by using a linear and an exponential equation of state. These results showed the pressure required to drive the flow for a given tube length is reduced with compressibility. Moreover, the two-dimensional axial velocity was characterized by pluglike regions the size of which increases upstream, in agreement with more sophisticated numerical simulations [26].

The objective of the present work is to extend the work of Taliadorou et al. [28] allowing slip at the wall. In order to investigate the combined effects of compressibility and slip, we solve approximately the plane and axisymmetric Poiseuille flows of weakly compressible fluids with yield stress, i.e. fluids obeying the Herschel–Bulkley constitutive equation, under the lubrication approximation assumptions used by Person and Denn [16] for power-law fluids. A linear equation of state relating the fluid density to the pressure is employed [7]. To account for slip, Navier's slip condition is assumed to hold at the wall and the interfacial yield stress is taken to be zero ($\tau_c = 0$). Moreover, the slip coefficient is allowed to be pressure dependent. Both a linear and an exponential model are employed to describe the pressure-dependence of the slip coefficient.

The paper is organized as follows. In Section 2, we summarize the solution of the one-dimensional incompressible axisymmetric Poiseuille flow of a Herschel–Bulkley fluid with Navier (i.e. pressure-independent linear) slip at the wall and discuss the underlying assumptions. In Section 3, the results are extended to the two-dimensional weakly compressible Poiseuille flow. Analytical and semi-analytical results are presented for both the incompressible and compressible flows and comparisons are made with avail-

able perturbation solutions. In Section 4, the case of pressure-dependent slip is analyzed and discussed. The equations for the planar compressible Poiseuille flow are given in Appendix A.

2. Incompressible Poiseuille flow with slip

The tensorial form of the constitutive equation of a compressible Herschel–Bulkley fluid with zero bulk viscosity (which implies that the viscosity forces are only due to shear and not to volume variations [26]) is:

$$\begin{cases} \dot{\gamma} = \mathbf{0}, & \tau \leqslant \tau_0 \\ \boldsymbol{\tau} = \left(\dfrac{\tau_0}{\dot{\gamma}} + k\dot{\gamma}^{n-1} \right) \left(\dot{\boldsymbol{\gamma}} - \dfrac{2}{3}\nabla \cdot \mathbf{u}\mathbf{I} \right), & \tau \geqslant \tau_0 \end{cases} \tag{8}$$

where $\boldsymbol{\tau}$ is the stress tensor, $\mathbf{u}$ is the velocity vector, $\mathbf{I}$ is the unit tensor, and $\dot{\boldsymbol{\gamma}}$ is the rate-of-strain tensor, i.e.

$$\dot{\boldsymbol{\gamma}} \equiv \nabla \mathbf{u} + (\nabla \mathbf{u})^T \tag{9}$$

where $\nabla \mathbf{u}$ is the velocity-gradient tensor, and the superscript T denotes its transpose. Moreover, k is the consistency index, n is the power law exponent, and $\dot{\gamma}$ and τ are respectively the magnitudes of $\dot{\boldsymbol{\gamma}}$ and $\boldsymbol{\tau}$, e.g.

$$\dot{\gamma} \equiv \sqrt{\frac{1}{2}II_{\dot{\gamma}}} = \sqrt{\frac{1}{2}\dot{\boldsymbol{\gamma}} : \dot{\boldsymbol{\gamma}}} \tag{10}$$

II being the second invariant of a tensor. The power-law fluid and the Bingham plastic are the special cases of the Herschel–Bulkley model for $\tau_0 = 0$ and $n = 1$, respectively.

In the present work, we consider the steady, laminar axisymmetric Poiseuille flow of a Herschel–Bulkley fluid in a tube of radius R, as shown in Fig. 1. We also assume that slip occurs along the wall according to Navier's slip Eq. (1). In Sections 2 and 3, the slip coefficient α is assumed to be constant. As already mentioned, the limiting case $\alpha \to \infty$ corresponds to full-slip, whereas $\alpha = 0$ corresponds to the no-slip boundary condition. In Section 4, we investigate the more general case where α varies with pressure.

The solution of the steady, incompressible Poiseuille flow of a Herschel–Bulkley fluid with slip at the wall is straightforward. This has been provided under different forms by Kalyon and co-workers [29]. It is presented here in order to show the analogy with the weakly compressible solution of Section 3 and to introduce the non-dimensionalization of the problem. Under the assumptions of unidirectionality and zero gravity, the z-momentum equation becomes

$$-\frac{dp}{dz} + \frac{1}{r}\frac{\partial}{\partial r}(r\tau_{rz}) = 0 \tag{11}$$

where the pressure gradient $(-dp/dz)$ is constant. The constitutive Eq. (11) is simplified as follows:

$$\begin{cases} \dfrac{\partial u_z}{\partial r} = 0, & |\tau_{rz}| \leqslant \tau_0 \\ \tau_{rz} = -\tau_0 - k\left(-\dfrac{\partial u_z}{\partial r} \right)^n, & |\tau_{rz}| \geqslant \tau_0 \end{cases} \tag{12}$$
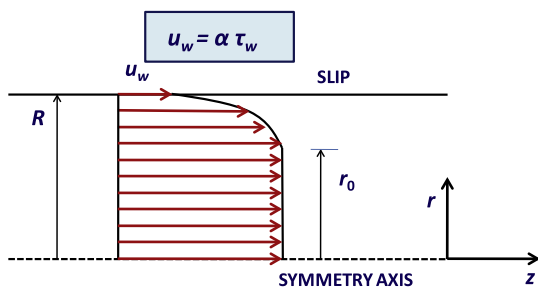

Fig. 1. Geometry of axisymmetric Poiseuille flow of a Herschel–Bulkley fluid.

The resulting axial velocity component is given by

$$u_z(r) = u_w + \frac{n}{2^{1/n}(n+1)k^{1/n}}\left(-\frac{dp}{dz} \right)^{1/n}$$
$$\times \begin{cases} (R - r_0)^{1/n+1}, & 0 \leqslant r \leqslant r_0 \\ \left[(R - r_0)^{1/n+1} - (r - r_0)^{1/n+1} \right], & r_0 \leqslant r \leqslant R \end{cases} \tag{13}$$

where u_w is the slip velocity, given by

$$u_w = \frac{\alpha R}{2}\left(-\frac{dp}{dz} \right) \tag{14}$$

and

$$r_0 = \frac{2\tau_0}{(-dp/dz)} < R \tag{15}$$

denotes the yield point, i.e. the point at which the material yields. Note that when $(-dp/dz) < 2\tau_0/R$ the fluid moves with uniform velocity u_w. The volumetric flow rate is given by

$$Q = \pi R^2 u_w + \frac{\pi n}{2^{1/n}(3n+1)k^{1/n}}\left(-\frac{dp}{dz} \right)^{1/n} R^{1/n+3}\left(1 - \frac{r_0}{R} \right)^{1/n+1}$$
$$\times \left\{ 1 + \frac{2n}{2n+1}\frac{r_0}{R}\left[1 + \frac{n}{n+1}\frac{r_0}{R} \right] \right\} \tag{16}$$

In what follows, it is preferable to work with dimensionless equations. We thus scale lengths by the tube radius, R, the velocity by the mean velocity, V_0, in the capillary, and the pressure and the stress components by $\frac{kV_0^n}{R^n}$. With these scalings, the dimensionless form of the slip equation is

$$\tau_w = \frac{1}{2A_1}u_w \tag{17}$$

where

$$A_1 \equiv \frac{k\alpha V_0^{n-1}}{2R^n} \tag{18}$$

is the slip number. The no-slip and full-slip limiting cases are recovered when $A_1 \to 0$ and ∞, respectively.

The dimensionless version of the constitutive equation, i.e. of Eq. (12), is:

$$\begin{cases} \dfrac{\partial u_z}{\partial r} = 0, & |\tau_{rz}| \leqslant Bn \\ \tau_{rz} = -Bn - \left(-\dfrac{\partial u_z}{\partial r} \right)^n, & |\tau_{rz}| \geqslant Bn \end{cases} \tag{19}$$

where

$$Bn \equiv \frac{\tau_0 R^n}{kV_0^n} \tag{20}$$

is the Bingham number. The dimensionless velocity profile is written as follows

$$u_z(r) = u_w + \frac{n}{2^{1/n}(n+1)}\left(-\frac{dp}{dz} \right)^{1/n}$$
$$\begin{cases} (1 - r_0)^{1/n+1}, & 0 \leqslant r \leqslant r_0 \\ \left[(1 - r_0)^{1/n+1} - (r - r_0)^{1/n+1} \right], & r_0 \leqslant r \leqslant 1 \end{cases} \tag{21}$$

where

$$u_w = A_1\left(-\frac{dp}{dz} \right) \tag{22}$$

and

$$r_0 = \frac{2Bn}{(-dp/dz)} \leqslant 1 \tag{23}$$

If $(-dp/dz) \leqslant 2Bn$, the fluid is sliding with uniform velocity u_w. Otherwise, the dimensionless pressure-gradient is a solution of the following equation:

$$2^{1/n} \frac{3n+1}{n} (1-u_w) \left(-\frac{dp}{dz} \right)^3 = \left[\left(-\frac{dp}{dz} \right) - 2Bn \right]^{1/n+1}$$
$$\times \left[\left(-\frac{dp}{dz} \right)^2 + \frac{4nBn}{2n+1} \left(-\frac{dp}{dz} \right) + \frac{8n^2Bn^2}{(n+1)(2n+1)} \right] \quad (24)$$

In the case of a Bingham plastic ($n = 1$) flow with slip at the wall, Eq. (24) is reduced to

$$3(1+8A_1)\left(-\frac{dp}{dz} \right)^4 - 8(Bn+3)\left(-\frac{dp}{dz} \right)^3 + 16Bn^4 = 0 \quad (25)$$

(a)

(b)

(c)
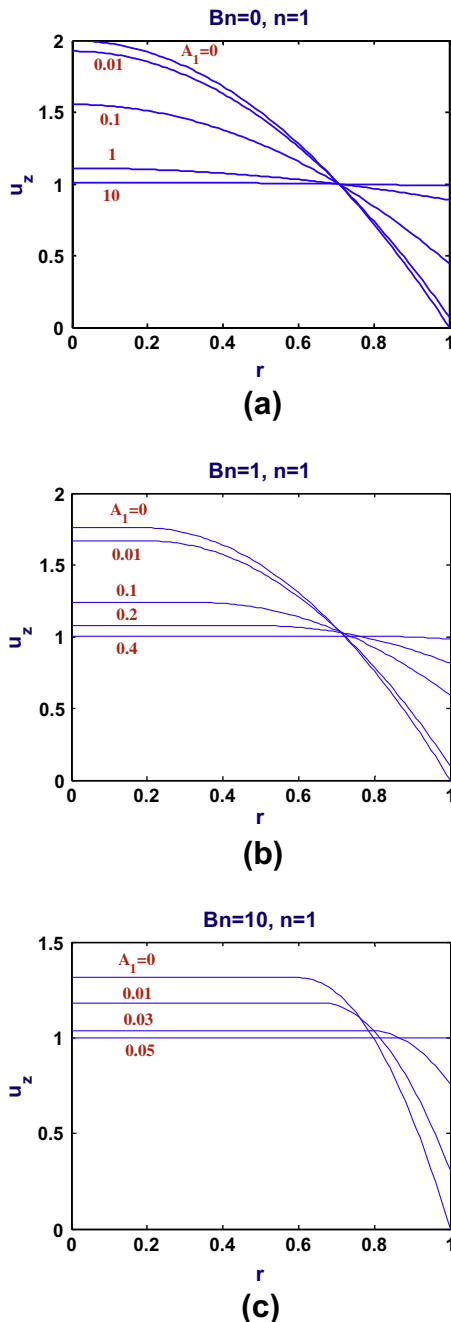
Fig. 2. Velocity profiles in incompressible flow with various values of the slip number: (a) Newtonian fluid; (b) Bingham fluid with $Bn = 1$ (the critical slip number is $A_{1,crit} = 0.5$); and (c) Bingham fluid with $Bn = 10$ (the critical slip number is $A_{1,crit} = 0.05$).

(a)

(b)
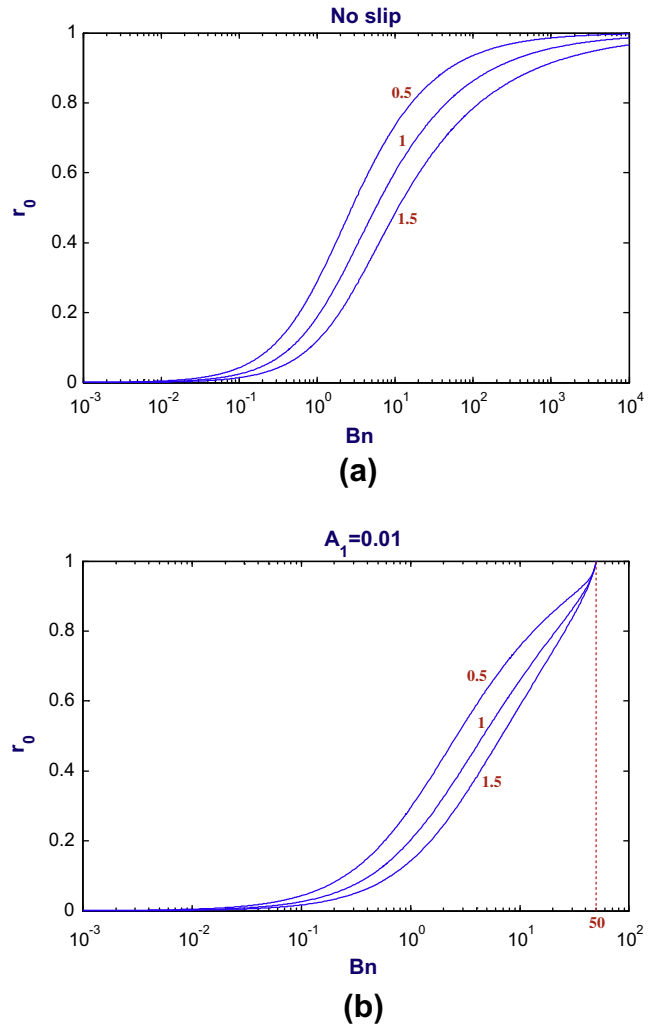
Fig. 3. Variation of the yield point in incompressible flow of a Herschel–Bulkley fluid for various values of the power-law exponent: (a) no slip and (b) slip with $A_1 = 0.01$ (the critical Bingham number is $Bn = 50$).
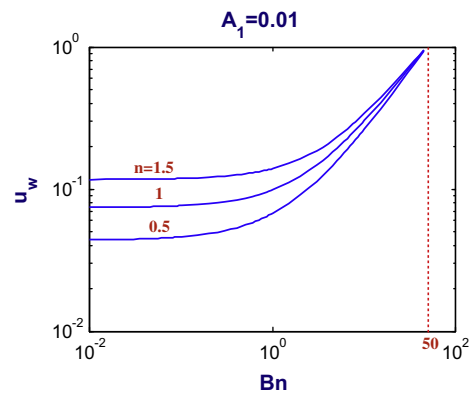
Fig. 4. Slip velocities for incompressible flow versus the Bingham number for different power-law exponents and $A_1 = 0.001$. Note that the critical Bingham number is 50.

In the case of the flow of a power-law fluid ($Bn = 0$), one gets:

$$2^{1/n} \frac{3n+1}{n} \left[1 - A_1 \left(-\frac{dp}{dz} \right) \right] = \left(-\frac{dp}{dz} \right)^{1/n} \quad (26)$$
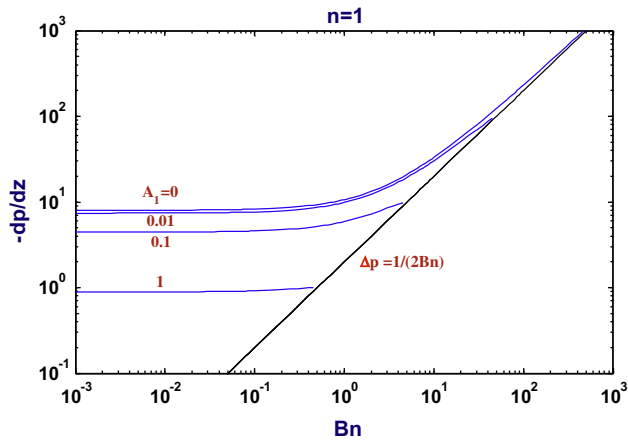
Fig. 5. Pressure gradient for incompressible flow versus the Bingham for different values of the slip number A_1 and $n = 1$. The critical value of the pressure gradient is $1/2Bn$.
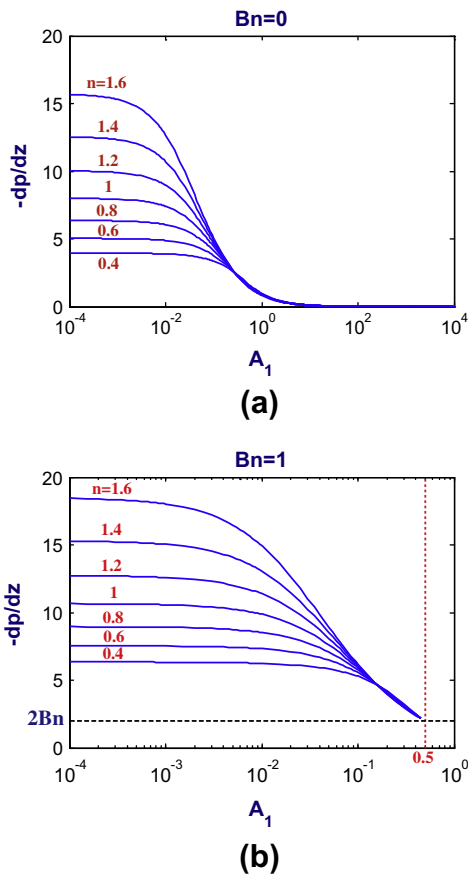

(a)

(b)

Fig. 6. Pressure gradient for incompressible flow versus the slip number A_1 for different values of the power-law exponent: (a) $Bn = 0$ (power-law fluid) and (b) $Bn = 1$; the critical value of A_1 is 0.5.

The above equation can be solved analytically only for certain values of the power-law exponent. For a Newtonian fluid ($n = 1$) the standard Poiseuille flow solution with slip is recovered:

$$\left(-\frac{dp}{dz}\right) = \frac{8}{1 + 8A_1} \quad \text{and} \quad p = -\frac{8z}{1 + 8A_1} \tag{27}$$

$$u_w = \frac{8A_1}{1 + 8A_1} \tag{28}$$

and

$$u_z(r) = \frac{8A_1 + 2(1 - r^2)}{1 + 8A_1} \tag{29}$$

Similarly, for $n = 1/2$ and $1/3$ one finds respectively

$$\left(-\frac{dp}{dz}\right) = 2\sqrt{5\left(1 + 5A_1^2\right)} - 10A_1 \tag{30}$$

and

$$\left(-\frac{dp}{dz}\right) = 2\left(\sqrt{64A_1^3 + 9} + 24\right)^{1/3} - \frac{8A_1}{\left(\sqrt{64A_1^3 + 9} + 24\right)^{1/3}} \tag{31}$$

The corresponding velocity profiles are then given as special cases of Eq. (21) (with $r_0 = 0$):

$$u_z(r) = A_1\left(-\frac{dp}{dz}\right) + \frac{n}{2^{1/n}(n + 1)}\left(-\frac{dp}{dz}\right)^{1/n}(1 - r^{1/n+1}) \tag{32}$$

In the general case, for any values of Bn, n, and A_1, the nonlinear Eq. (24) is easily solved for the pressure gradient, and then the velocity profile can be calculated by means of Eq. (21). In Fig. 2, the velocity profiles of a Newtonian ($Bn = 0$) and two Bingham fluids ($Bn = 1$ and 10) are shown for various values of the slip number. With the Newtonian fluid, the velocity tends to a plug profile ($u_x = u_w = 1$) in the limit of infinite A_1 (full slip). Interestingly, with viscoplastic fluids, the plug velocity profile is attained at a finite value of A_1 at which the yield distance r_0 becomes 1. This phenomenon is illustrated in Fig. 3, where the yield distances for $n = 0.5$, 1, and 1.5 are plotted versus the Bingham number. We observe that the
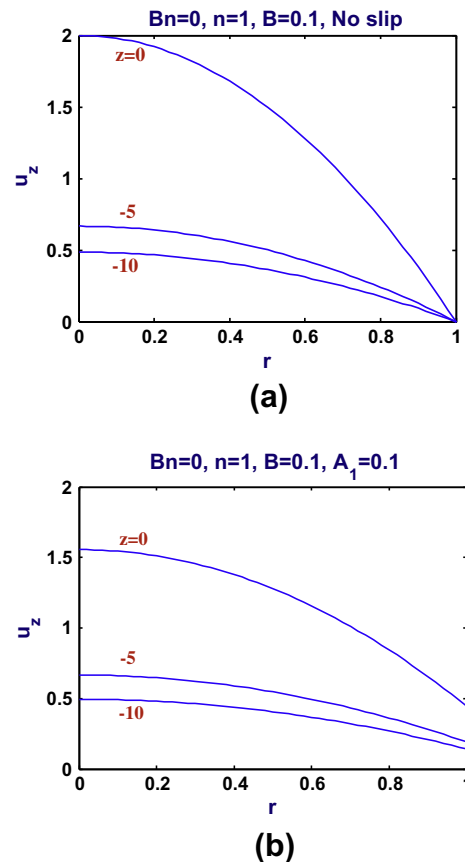

(a)

(b)

Fig. 7. Velocity profiles across the tube in compressible Newtonian flow with $B = 0.1$: (a) no slip ($A_1 = 0$) and (b) pressure-independent slip ($A_1 = 0.1$).
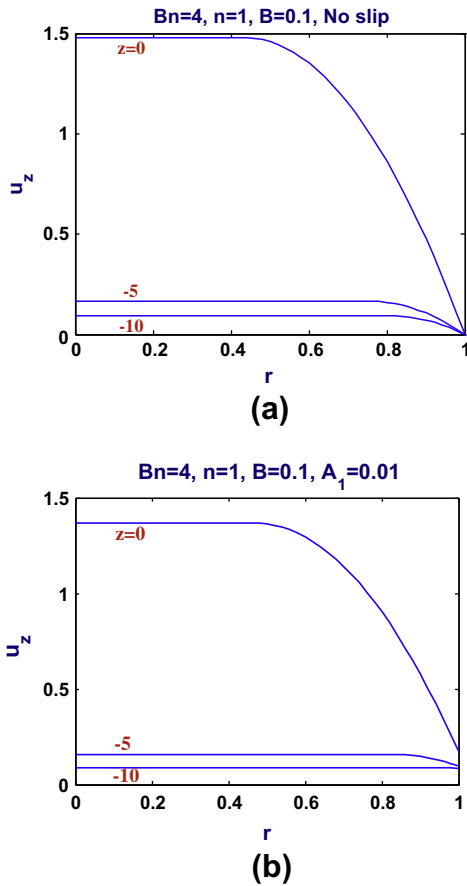
(a)

(b)

Fig. 8. Velocity profiles across the tube in compressible Bingham flow with $Bn = 4$ and $B = 0.1$: (a) no slip ($A_1 = 0$) and (b) pressure-independent slip ($A_1 = 0.01$).
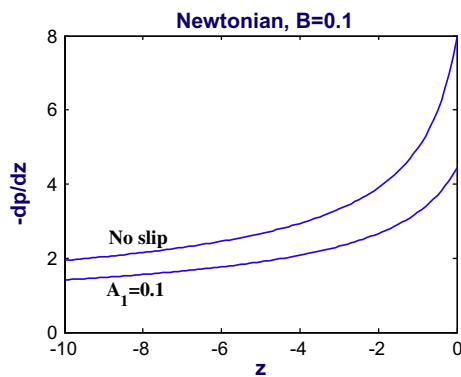

Fig. 9. Variation of the pressure gradient within the tube in the case of a compressible Newtonian fluid with $B = 0.1$ and $L = 10$.

size of the yielded region is reduced as the power-law exponent is increased. When no-slip is applied (Fig. 3a), r_0 tends to unity asymptotically as Bn goes to infinity. When slip occurs (Fig. 3b), r_0 becomes 1 and the velocity profile is plug at a critical Bingham number, the value of which is independent of the power-law exponent n. In other words, the flow becomes plug at a critical wall shear stress, which agrees, for example, with experimental observations on highly filled suspensions [13].

It is clear that when Navier slip with zero slip yield stress is allowed, for a given value of A_1 there is an upper bound for the Bingham number at which both the yield distance and the slip velocity

become 1 (Fig. 4). Equivalently, for a given Bingham number, solutions beyond a critical value of A_1 are not admissible. Note that for values of A_1 above a critical value the LHS of Eq. (24) becomes negative while the RHS is always positive, since $(-dp/dz) > 2Bn$. The critical value of A_1 at which both sides of Eq. (24) vanish is

$$A_{1,crit} = \frac{1}{\left(-\frac{dp}{dz}\right)_{crit}} = \frac{1}{2Bn} \tag{33}$$

Similarly, a critical Bingham number is defined when the value of the slip number is specified. Theoretically, there can be plug flow in the limiting case $(-dp/dz) = 2Bn$ when linear slip is allowed and the slip number is given by Eq. (33). Fig. 4 also illustrates the variation of the slip velocity with the Bingham number. A plateau is observed initially corresponding to essentially Newtonian flow, but then u_w increases rapidly reaching unity at the corresponding critical Bingham number.

The combined effects of the Bingham and slip numbers on the pressure gradient required to drive the flow are illustrated in Fig. 5. As the slip number is increased, the dependence of the pressure gradient on Bn and the corresponding critical Bingham number are reduced. Finally, Fig. 6 shows plots of the pressure gradient for $Bn = 0$ and 1 and various values of the exponent n. Obviously, the required pressure gradient increases with n. All curves are horizontal initially but as slip becomes stronger, $(-dp/dz)$ decreases rapidly. In the case of a power-law fluid, it goes asymptotically to zero, whereas in the case of a yield-stress fluid it goes down to the critical value $2Bn$ at a finite value of the slip number.

The above remarks for the existence of a finite critical slip number hold only when the interfacial yield stress is zero. If, for exam-
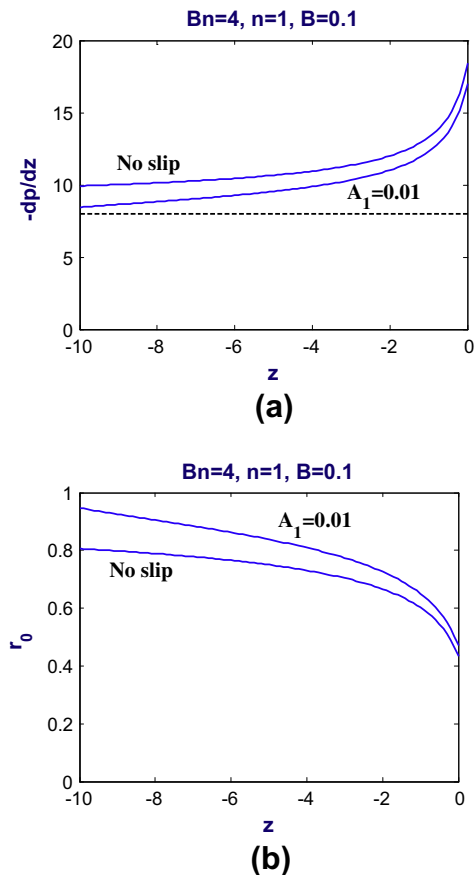

(a)

(b)

Fig. 10. Variation of (a) the pressure gradient and (b) the yield point within the tube in the case of a compressible Bingham fluid with $Bn = 4$, $B = 0.1$, and $L = 10$.

ple, $\tau_c = \tau_0$ and slip is described by Eq. (5) with $m = 1$, then the dimensionless slip velocity in axisymmetric Poiseuille flow when $\tau_w > \tau_0$ is given by

$$u_w = A_1\left[\left(-\frac{dp}{dz}\right) - 2Bn\right] \tag{34}$$

and, thus,

$$A_{1,crit} = \frac{1}{\left[\left(-\frac{dp}{dz}\right) - 2Bn\right]_{crit}} \to \infty \tag{35}$$

The analysis of flow in the case of non-zero slip yield stress is out of the scope of the present work.

3. Weakly compressible Poiseuille flow with slip

For a weakly compressible flow, it can be assumed that the radial velocity component is zero. This assumption is consistent up to first order with Newtonian perturbation solutions in terms of compressibility [30]. Assuming further that $\partial u_z/\partial z \ll 1$, then $\dot{\gamma} \approx |\partial u_z/\partial r|$. In creeping flow, the z-momentum equation is reduced to Eq. (11) where the pressure gradient is now a function of z. These assumptions are valid in very long tubes, i.e. when $R/L \ll 1$ [26]. With the terminology of Wachs et al. [31] the present model is a 1.5D model. However, this can simply be viewed as a lubrication approximation model [16]. Being a function of the pres-

sure, the density also varies across the tube, i.e. $\rho = \rho(z)$. For the mass to be conserved, there must be

$$\rho(z)Q(z) = Q_0 \tag{36}$$

where $Q(z)$ is the volumetric flow rate and $Q_0 = Q(0)$. The dimensionless axial velocity (scaled by the mean velocity, V_0, at the exit of the capillary) is then given by

$$u_z(r,z) = A_1\left(-\frac{dp}{dz}\right)(z) + \frac{n}{2^{1/n}(n+1)}\left(-\frac{dp}{dz}\right)^{1/n}(z)$$
$$\begin{cases} (1 - r_0(z))^{1/n+1}, & 0 \leqslant r \leqslant r_0 \\ \left[(1 - r_0(z))^{1/n+1} - (r - r_0(z))^{1/n+1}\right], & r_0 \leqslant r \leqslant 1 \end{cases} \tag{37}$$

where r_0 is now a function of z:

$$r_0(z) = \frac{2Bn}{(-dp/dz)(z)} < 1 \tag{38}$$

It is clear that at the capillary exit ($z = 0$), Eqs. (37) and (38) yield the incompressible flow solution.

As pointed out by Vinay et al. [26], $r_0(z)$ in steady compressible Poiseuille flow is just a pseudo-yield point, i.e. a convenient idealization. Since the axial velocity varies along the tube, $\partial u_z/\partial z > 0$ and thus $\dot{\gamma}$ is nonzero, which implies that unyielded regions, similar to the classical plug regions, cannot be obtained. Vinay et al. [26] have also calculated steady-state velocity profiles at the inlet and the outlet of the tube with the plug region at the center corresponding to half the pipe radius.

The pressure dependence of the density is taken into account by means of a linear thermodynamic equation of state. At constant
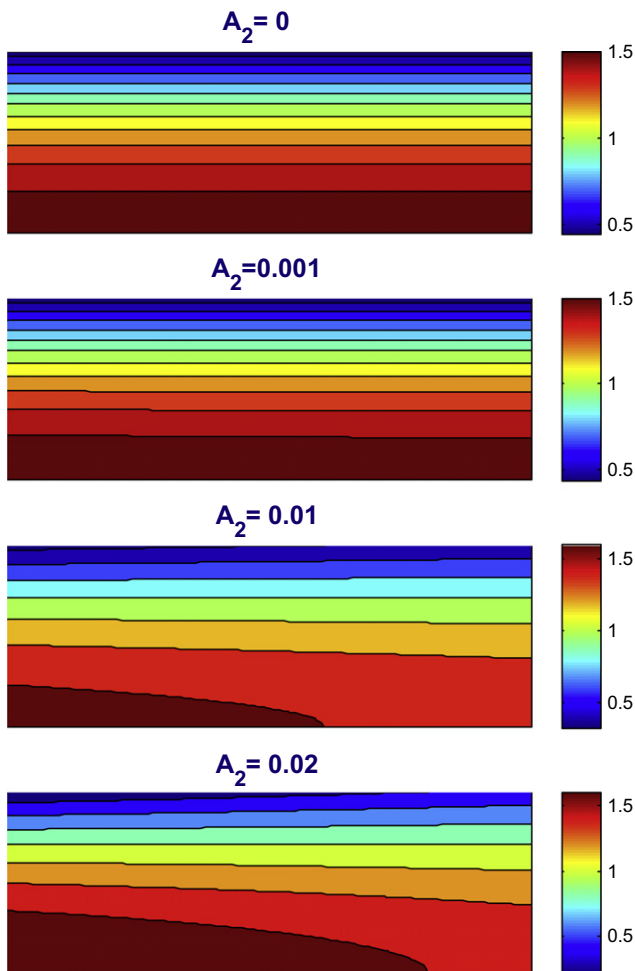
Fig. 11. Velocity contours in incompressible Newtonian flow with pressure-dependent slip for $A_1 = 0.1$ and various values of A_2 (exponential model); $L = 10$.
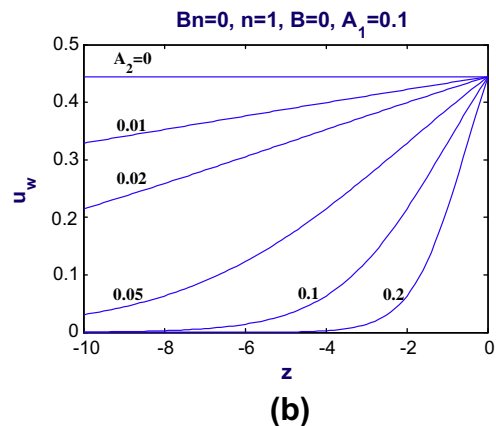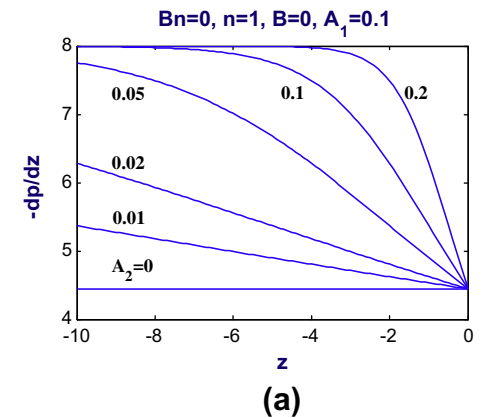
Fig. 12. Pressure gradient (a) and slip velocity (b) in incompressible Newtonian flow with pressure-dependent slip for $A_1 = 0.1$ and various values of A_2 (exponential model); $L = 10$.
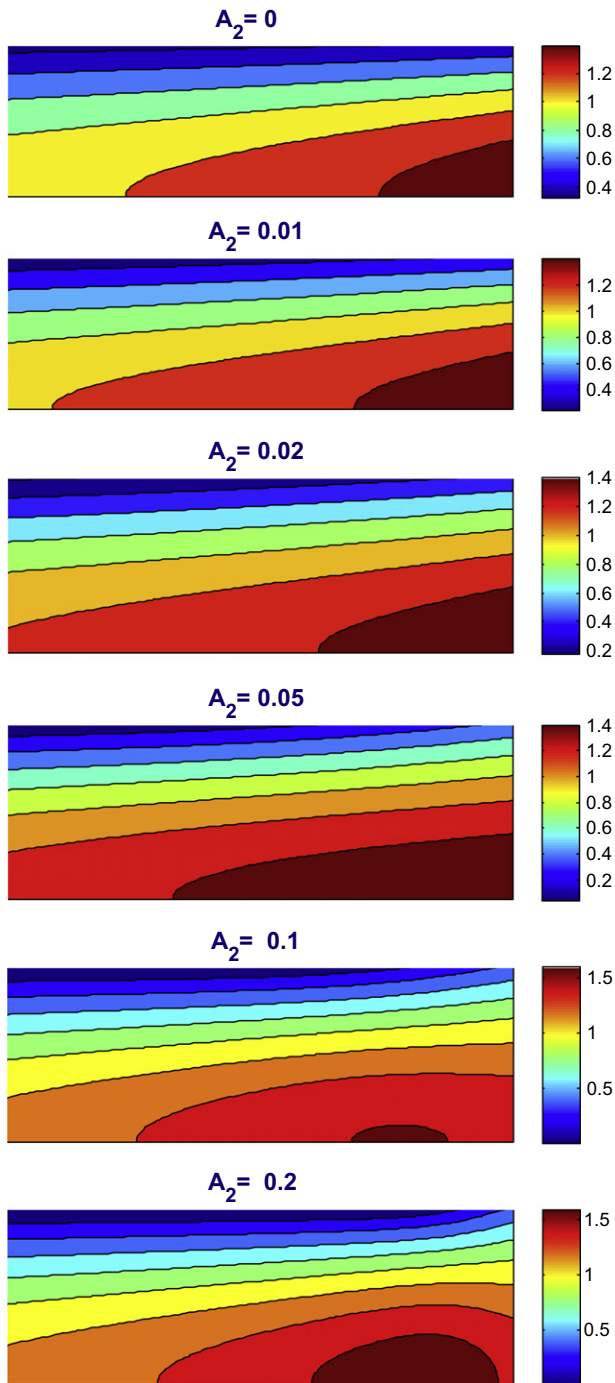
Fig. 13. Velocity contours in compressible Newtonian flow with pressure-dependent slip for $B = 0.01$, $A_1 = 0.1$ and various values of A_2 (exponential model); $L = 10$.

temperature and for low pressures, the density can be represented by the linear approximation of the standard exponential expression:

$$\rho = \rho_0[1 + \beta(p - p_0)] \tag{39}$$

where $\beta \equiv -(\partial v/\partial p)_{p_0,T_0}/v_0$ is the isothermal compressibility assumed to be constant, v is the specific volume, ρ_0 and v_0 are, respectively, the density and the specific volume at the reference pressure p_0, and temperature, T_0. The equation of state is nondimensionalized scaling the density ρ by ρ_0 and the pressure as in Section 2:

$$\rho = 1 + Bp \tag{40}$$

where the reference pressure, p_0, has been set to zero, and B is the compressibility number,

$$B \equiv \frac{\beta k V_0^n}{R^n} \tag{41}$$

The pressure gradient $(-dp/dz)(z)$ across the capillary, i.e. for $z \leqslant 0$, can be calculated using the conservation of mass, i.e. Eq. (36). It turns out that the pressure gradient is a solution of the following equation

$$2^{1/n}\frac{3n+1}{n}\left(-\frac{dp}{dz}\right)^3\left[\frac{1}{\rho(p)} - u_w\right] = \left[\left(-\frac{dp}{dz}\right) - 2Bn\right]^{1/n+1}$$
$$\left[\left(-\frac{dp}{dz}\right)^2 + \frac{4nBn}{2n+1}\left(-\frac{dp}{dz}\right) + \frac{8n^2Bn^2}{(n+1)(2n+1)}\right] \tag{42}$$

which involves the pressure-dependent density of the fluid. The pressure gradient can be viewed as a function of p and is expected to decrease upstream.

Eq. (42) can be integrated analytically and solved for p only in the case of a Newtonian fluid ($Bn = 0$, $n = 1$). It turns out that
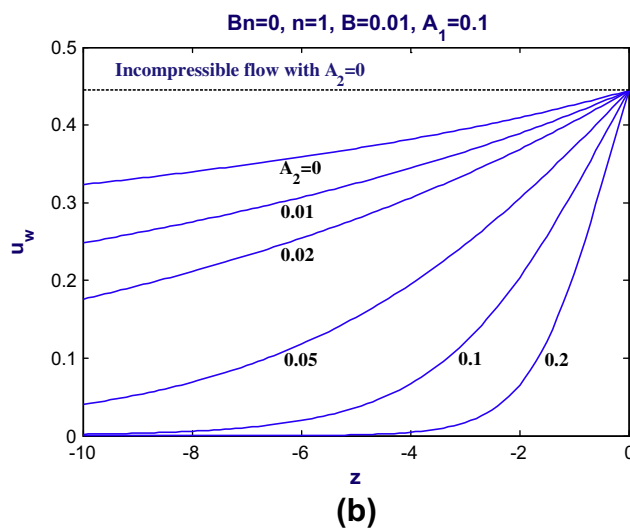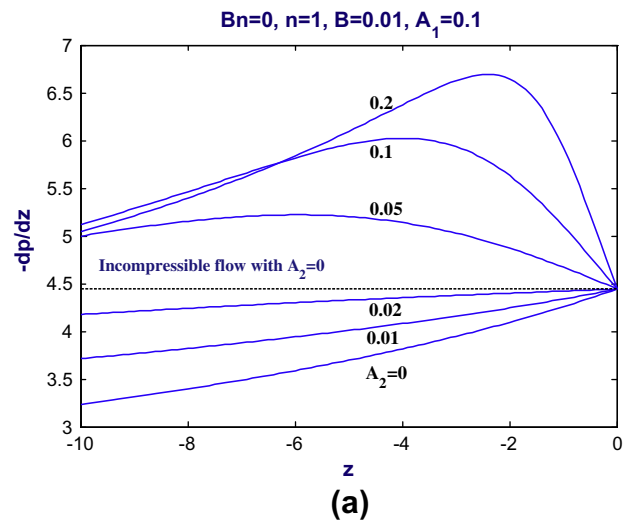

Fig. 14. Pressure gradient (a) and slip velocity (b) in compressible Newtonian flow with pressure-dependent slip for $B = 0.01$, $A_1 = 0.1$ and various values of A_2 (exponential model); $L = 10$.
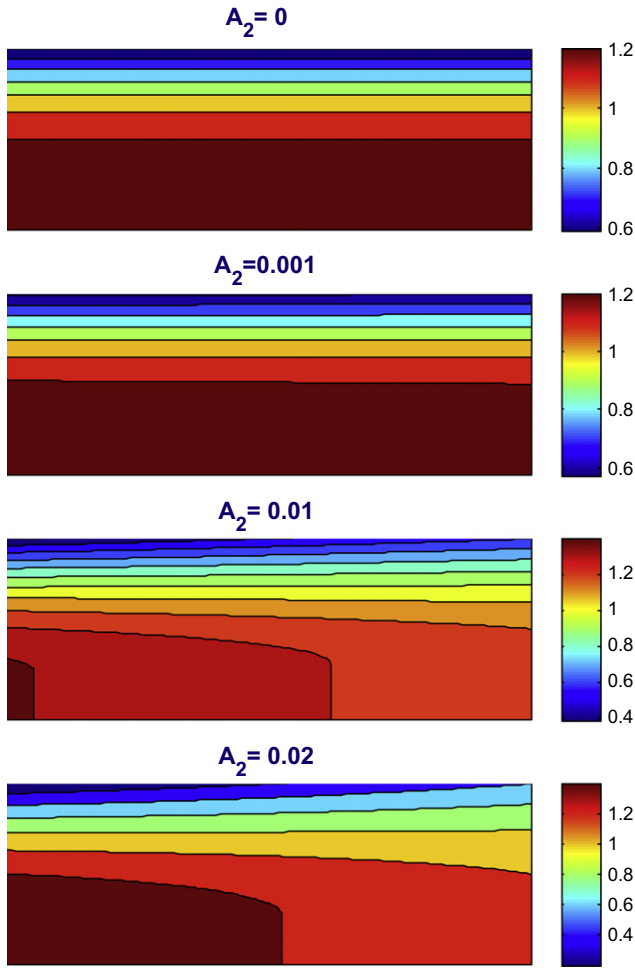
Fig. 15. Velocity contours in incompressible Bingham flow with pressure-dependent slip for $Bn = 1$, $A_1 = 0.1$ and various values of A_2 (exponential model); $L = 10$.

$$p(z) = \frac{1}{B}\left(\sqrt{1 - \frac{16}{1 + 8A_1}Bz} - 1\right) \qquad (43)$$

and the corresponding velocity profile is:

$$u_z(r, z) = \frac{8A_1 + 2(1 - r^2)}{(1 + 8A_1)\sqrt{1 - \frac{16}{1+8A_1}Bz}} \qquad (44)$$

The slip velocity is obviously given by

$$u_w(z) = \frac{8A_1}{(1 + 8A_1)\sqrt{1 - \frac{16}{1+8A_1}Bz}} \qquad (45)$$

The results in (43)–(45) agree with the perturbation solution of Poyiadji et al. [32] up to first order.

In the general case, the pressure gradient and the pressure are calculated numerically. Once the pressure $p(z)$ is known at a point (e.g., $p(0) = 0$), the pressure gradient $(-dp/dz)(z)$ can be calculated from Eq. (42). Then the pressure can be calculated by setting $p = 0$ at the exit plane ($z = 0$) and integrating the pressure gradient moving upstream [28].

The effect of compressibility on the shape of the velocity profile across the tube in the case of slip is illustrated in Figs. 7 and 8 for $Bn = 0$ (Newtonian) and 4 (Bingham plastic), where B was set to the rather high value of 0.1 in order to exaggerate compressibility effects. As for the slip coefficient, the value $A_1 = 0.1$ was used for

$Bn = 0$; for $Bn = 4$ a much lower value was used ($A_1 = 0.01$), for reasons to be discussed below. Due to compressibility, the mean velocity is reduced upstream. When slip occurs the radial dependence of the solution is weaker and the velocity profile tends to become flat. This effect becomes more striking in the case of Bingham fluids (Fig. 8). The pressure gradients across the tube for the two flows of Figs. 7 and 8 are plotted in Fig. 9 and Fig. 10a. As demonstrated by Taliadorou et al. [28] for the no-slip case, in compressible flow the pseudo-yield point moves towards the wall upstream. This phenomenon is accelerated by slip, as illustrated in Fig. 10b, where the variation of $r_0(z)$ across the tube is shown. In the case of no slip, the pseudo-yield point moves to the wall asymptotically. In the case of slip and under our assumptions the
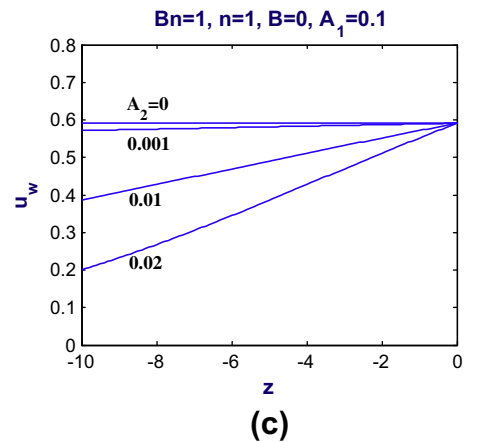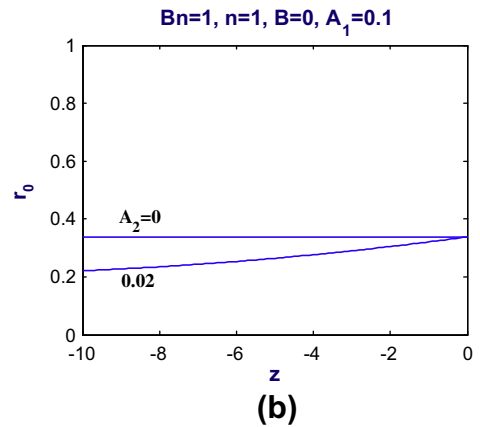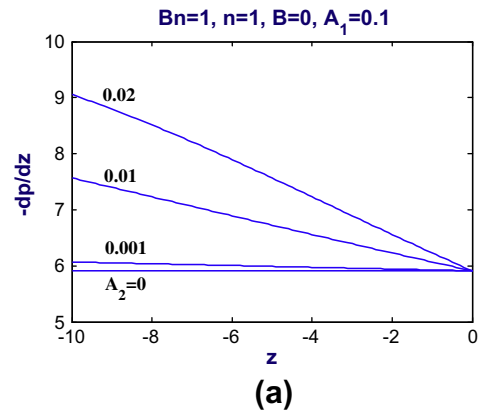

Fig. 16. Pressure gradient (a), yield point position (b), and slip velocity (c) in incompressible Bingham flow with pressure-dependent slip for $Bn = 1$, $A_1 = 0.1$ and various values of A_2 (exponential model); $L = 10$.

flow becomes plug at a finite distance upstream the exit. Similarly, the pressure gradient is reduced down to the critical value $2Bn$.

4. Poiseuille flows with pressure-dependent slip

In the case that the slip coefficient is pressure dependent, the above analysis still holds under the assumptions $u_y = 0$ and $\partial u_z / \partial z \ll 1$, with A_1 in Eq. (22) now replaced by a function of pressure, $A(p)$. As already mentioned, the analysis of Person and Denn [16] for the flow of a power-law fluid in a slit with pressure-dependent wall slip is based on the same assumptions (lubrication approximation). For a Newtonian fluid ($Bn = 0$ and $n = 1$), one gets:

$$\rho(p)[1 + 8A(p)]\left(-\frac{dp}{dz}\right) = 8 \tag{46}$$

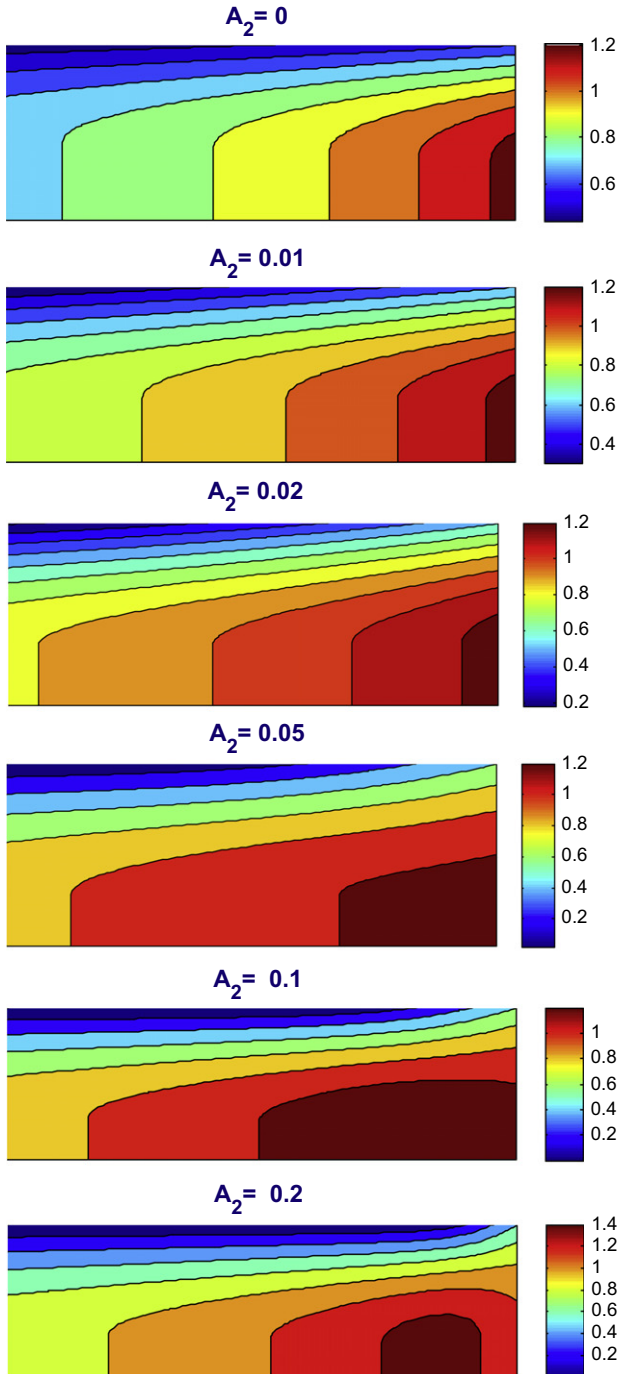which results in the following expression for the velocity profile:

Fig. 17. Velocity contours in compressible Bingham flow with pressure-dependent slip for $Bn = 1$, $B = 0.01$, $A_1 = 0.1$ and various values of A_2 (exponential model); $L = 10$.
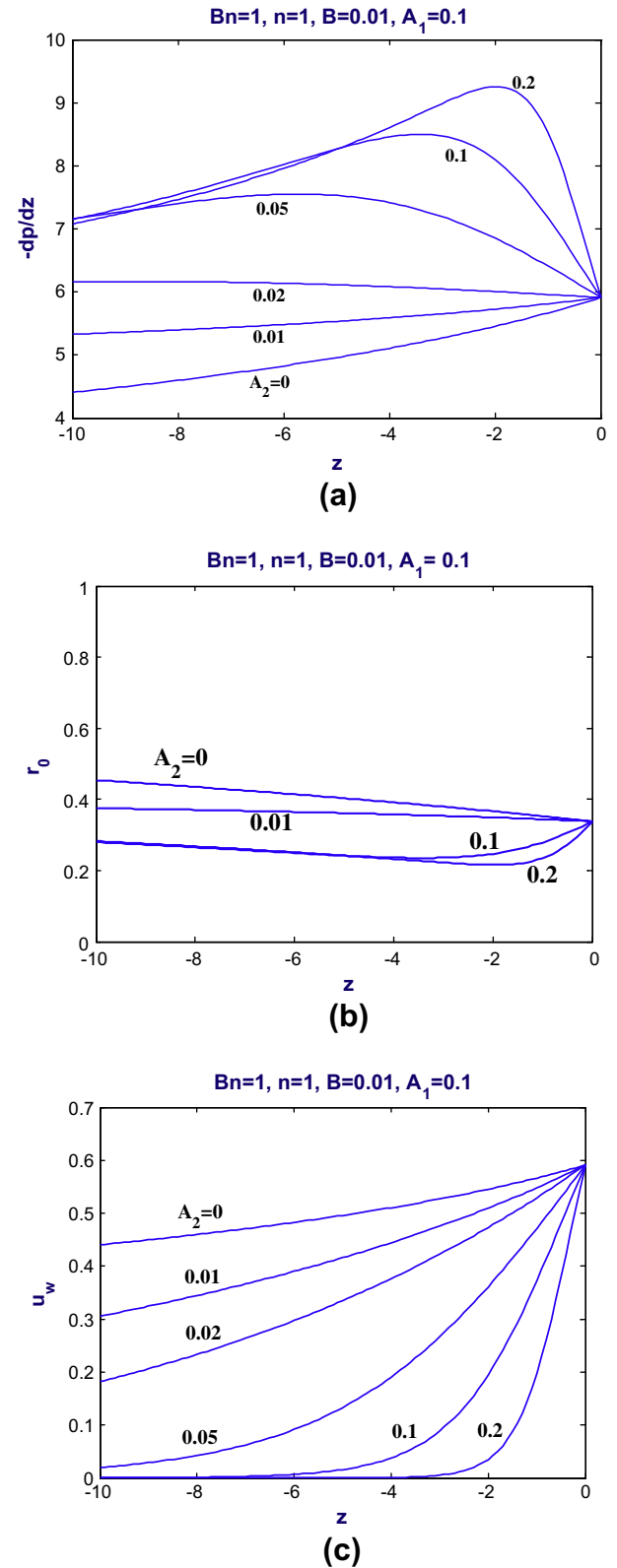

Fig. 18. Pressure gradient (a), yield point position (b), and slip velocity (c) in compressible Bingham flow with pressure-dependent slip for $Bn = 1$, $B = 0.01$, $A_1 = 0.1$ and various values of A_2 (exponential model); $L = 10$.

$$u_z(r,z) = \frac{8A(p) + 2(1 - r^2)}{\rho(p)[1 + 8A(p)]} \tag{47}$$

In the present work we considered two models describing the pressure dependence of A. The first is linear

$$A(p) = A_1 - A_2 p, \qquad 0 \leqslant p \leqslant A_1/A_2 \tag{48}$$

while the second one is exponential [16]:

$$A(p) = A_1 e^{-A_2 p} \tag{49}$$

where A_2 is a dimensionless constant:

$$A_2 \equiv \frac{k\alpha_2 V_0^n}{R^n} \tag{50}$$

Obviously when $A_2 = 0$, the pressure-independent Navier slip condition is recovered in both cases. The two models are equivalent for small values of A_2 and small pressures.

Substituting Eqs. (40) and (48) into Eq. (46) we get

$$(1 + Bp)[1 + 8A_1 - 8A_2 p]\left(-\frac{dp}{dz}\right) = 8 \tag{51}$$

From the above equation it is directly deduced that the effect of pressure-dependent slip is opposite to that of compressibility. Integrating Eq. (51) results in a cubic equation that can be solved analytically for the pressure p. In the case of incompressible flow ($B = 0$) one gets:

$$p(z) = \frac{1 + 8A_1}{8A_2}\left(1 - \sqrt{1 + \frac{128A_2}{(1 + 8A_1)^2}z}\right) \tag{52}$$

and

$$u_z(r,z) = \frac{8(A_1 - A_2 p) + 2(1 - r^2)}{(1 + 8A_1)\sqrt{1 + \frac{128A_2}{(1+8A_1)^2}z}} \tag{53}$$
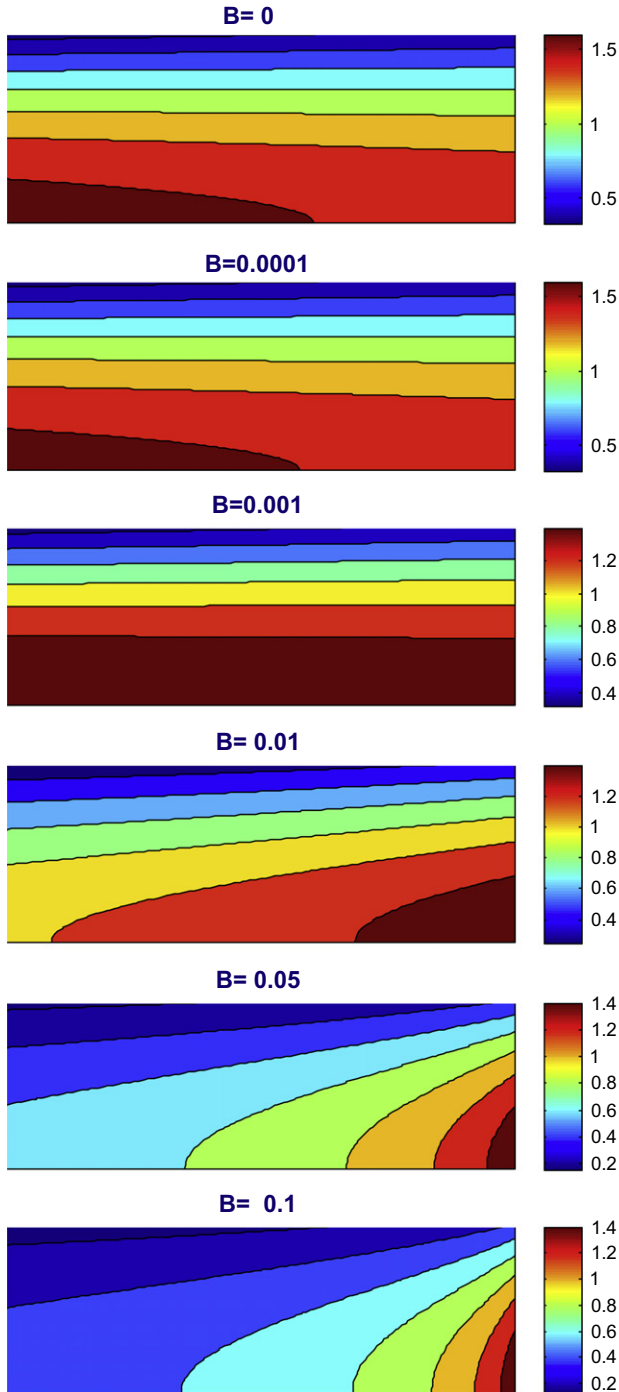

Fig. 19. Velocity contours in Newtonian flow with pressure-dependent slip for various compressibility numbers; $A_1 = 0.1$, $A_2 = 0.01$ (exponential model), and $L = 10$.
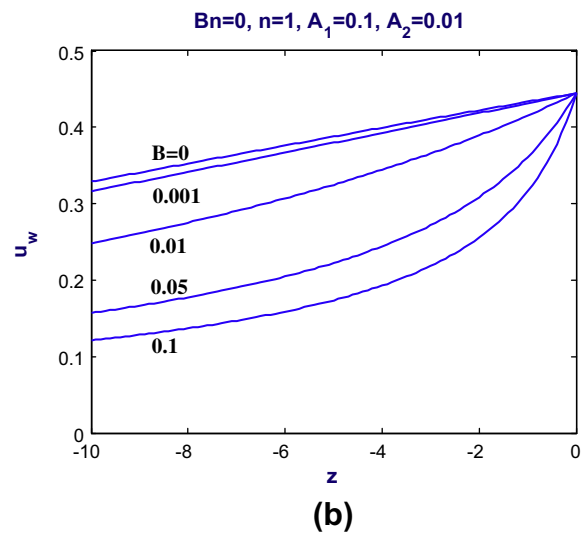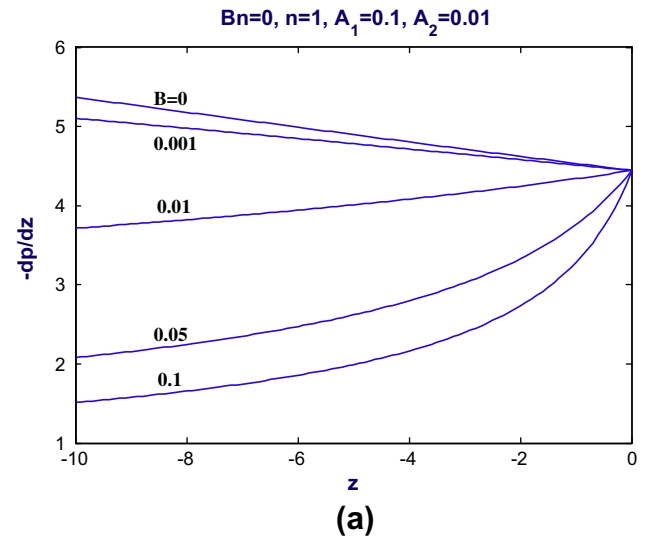

Fig. 20. Pressure gradient (a) and slip velocity (b) in Newtonian flow with pressure-dependent slip for various compressibility numbers; $A_1 = 0.1$, $A_2 = 0.01$ (exponential model), and $L = 10$.

The numerical results presented below have been obtained using the exponential model in Eq. (49), with which no analytical solution can be obtained. The velocity contours in incompressible Newtonian flow for $A_1 = 0.1$ and various values of A_2 are given in Fig. 11. For zero or small values of A_2 the contour lines are horizontal indicating that the flow is essentially one-dimensional. At higher values of A_2 the dependence of u_z on z becomes stronger and thus the contours are bending towards the axis of symmetry. Fig. 12 shows the profiles of the pressure gradient and the slip velocity across the tube for $A_1 = 0.1$ and various values of A_2. Obviously, for $A_2 = 0$ (no pressure-dependence) both the pressure gradient and the slip velocity are constant, since the flow is one-dimensional. For small values of A_2 (weak pressure-dependence), the pressure gradient decreases and the slip velocity increases linearly across the tube. For high values of A_2 (strong pressure dependence), slip is restricted only near the exit of the tube. Upstream, the slip velocity is essentially zero and the pressure gradient is constant.

The combined effects of compressibility and pressure-dependent slip for the Newtonian case are illustrated in Fig. 13, where the velocity contours for $B = 0.01$, $A_1 = 0.1$ and various values of A_2 are shown. As the pressure dependence is increased, the velocity contours tend to become horizontal and a velocity peak appears close to the tube exit. The variation of the pressure gradient and the slip velocity with A_2 is illustrated in Fig. 14. Note that due to compressibility both the pressure gradient and the slip velocity are increasing with the axial distance when $A_2 = 0$. As expected, the slip velocity is reduced and the pressure gradient increases with A_2. At high values of A_2, however, there appears a maximum

of the pressure gradient which moves towards the exit as A_2 is increased and slip becomes more localized.

The effects of the slip decay parameter A_2 in the case of Bingham flow are illustrated in Figs. 15–18, where velocity contours and results for the pressure gradient, the yield point, and the slip velocity are presented for both the incompressible and compressible cases. In incompressible flow ($B = 0.01$), the size of the pseudo-unyielded region is reduced upstream as the slip velocity is reduced (Figs. 15 and 16 for $Bn = 1$ and $B = 0$). In the compressible case, the results are more interesting, since at high values of A_2 the radius of the pseudo-unyielded region appears to pass through a minimum (Fig. 18) leading to the appearance of unyielded islands (Fig. 17). This phenomenon becomes more pronounced as the Bingham number is increased.

To investigate further the combined effects of slip pressure-dependency and compressibility, we fixed the slip parameters to $A_1 = 0.1$ and $A_2 = 0.01$ (always for the exponential model) and varied the compressibility number. It should be noted that the velocity profile at the exit plane ($z = 0$) is independent of the compressibility number, since this is by assumption the profile for incompressible flow with constant slip. In Fig. 19, a reversal of the velocity contour pattern is observed as the compressibility number is increased. Initially, the effects of the slip pressure-dependency prevail but as B is increased these are counterbalanced and then suppressed by compressibility effects. For $B = 0.001$ the competing effects of A_2 and B are equivalent so that the velocity contours are almost everywhere horizontal. The corresponding pressure-gradient and slip velocity distributions are given in Fig. 20. We observe in Fig. 20a that for small compressibility num-
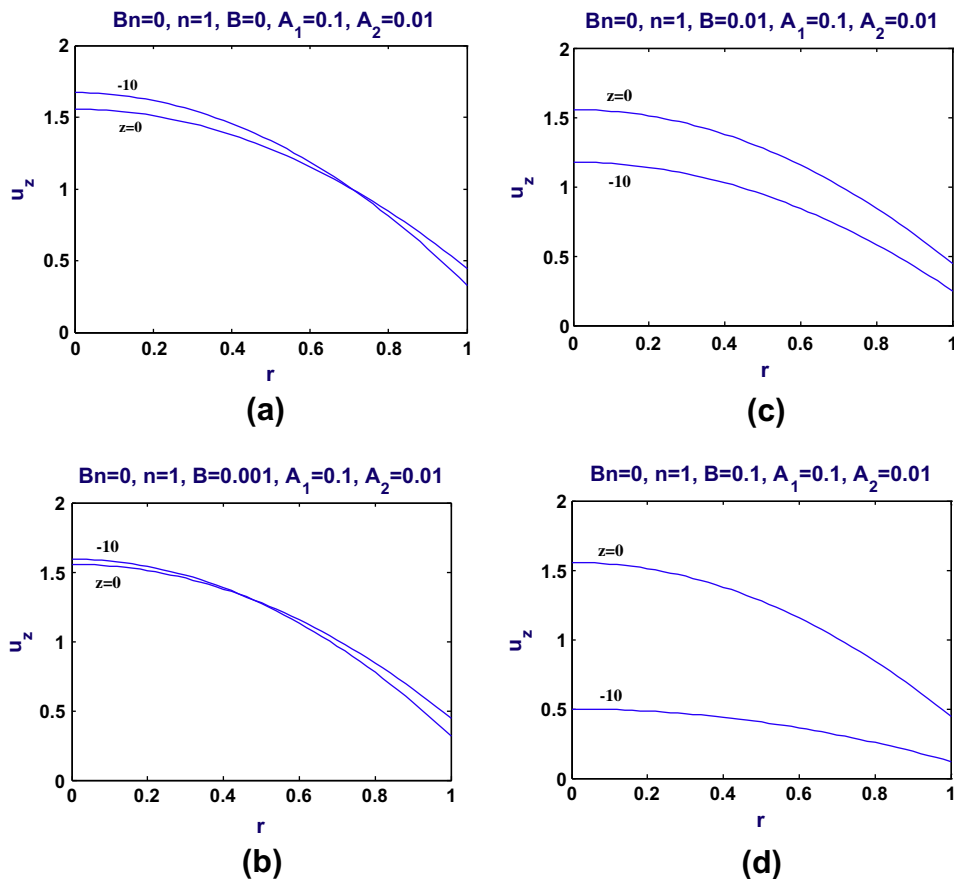

Fig. 21. Velocity profiles at the inlet and the outlet in Newtonian flow with pressure-dependent slip for $A_1 = 0.1$, $A_2 = 0.01$ (exponential model) and various compressibility numbers; $L = 10$

bers the pressure gradient is decreasing across the tube. However, this trend changes as B increases. For a critical value between 0.001 and 0.01 the pressure gradient is roughly constant and the velocity profile is weakly dependent on z. This effect is illustrated in Fig. 21 where the velocity profiles at the inlet and the outlet are compared for $B = 0$, 0.001, 0.01, and 0.1. As expected, the mean velocity is reduced upstream due to the conservation of mass. At some low value of B (Fig. 21b) the velocity profiles at the inlet and the outlet are quite similar, but at higher values of B the velocity at the inlet is reduced dramatically and tends to become flat. This phenomenon

becomes more striking in the case of Bingham flow in which the velocity in the unyielded region is flat anyway. In Fig. 22, we show results obtained with $Bn = 1$, $A_1 = 0.1$ and $A_2 = 0.01$. As in the Newtonian case, the velocity contour pattern changes dramatically as compressibility is increased. For small compressibility numbers, the pseudo-yield distance is slightly reduced upstream, but at higher compressibility numbers this trend is reversed. As in the case of pressure-independent slip, the flow upstream tends to become plug when the compressibility of the fluid is taken into account.
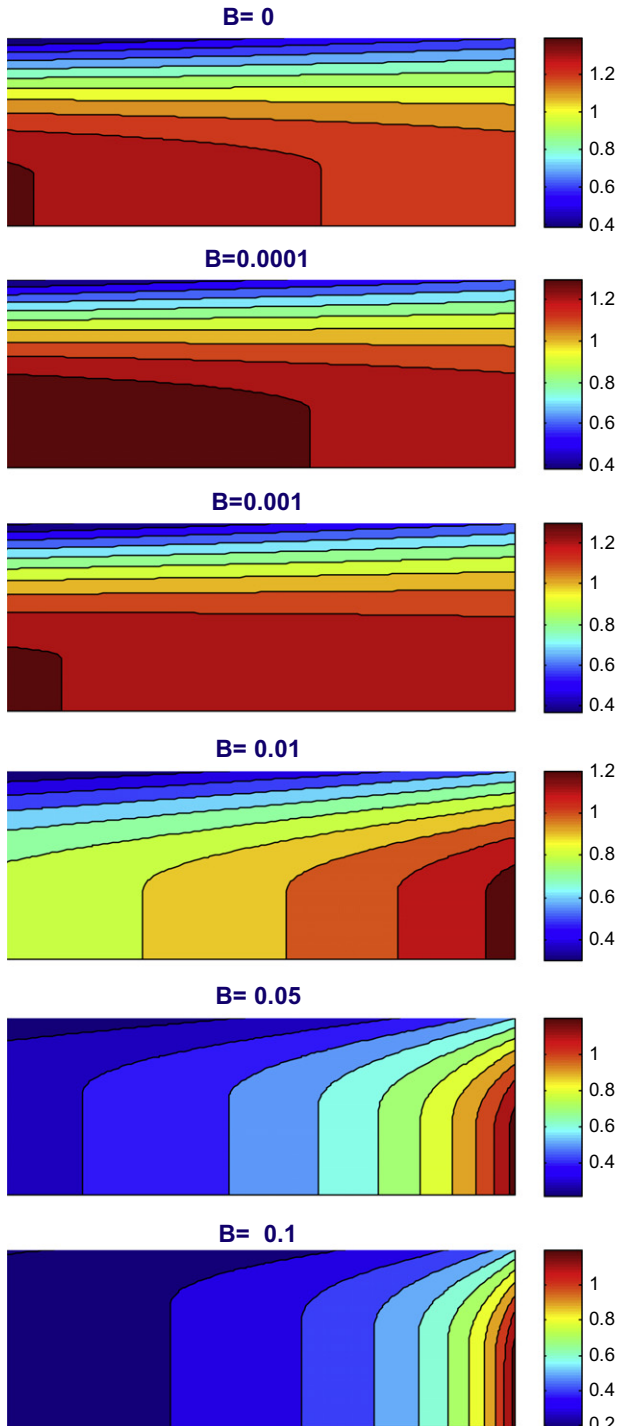
5. Conclusions

Approximate semi-analytical solutions of the steady, creeping, weakly compressible plane and axisymmetric Poiseuille flows of a Herschel–Bulkley fluid with slip at the wall have been derived, under lubrication approximation assumptions, employing a linear equation of state and Navier's slip condition with zero slip yield stress. The combined effects of compressibility, slip, and yield stress and the case of pressure-dependent slip have been investigated. In agreement with previous works [26,28], it was shown that when slip is present and the yield stress fluid is compressible, the velocity upstream, tends to become plug, which justifies the use of averaged models in solving viscoplastic flows in long tubes. This effect is enhanced with the presence of slip. It has also been demonstrated that the effect of slip pressure-dependency is opposite to that of compressibility. As for the future plans, we intend to extend the present analysis to 1.5D time-dependent models.

Appendix A. Compressible plane Poiseuille flow with slip

In plane Poiseuille flow, lengths are scaled by the channel-half-width, H, the velocity by the mean velocity, V_0, at the exit of the channel, and the pressure by kV_0/H^n. Under the same assumptions used for the axisymmetric flow, the dimensionless velocity profile in the case of compressible plane flow is written as follows:

$$u_x(x,y) = u_w(x) + \frac{n}{n+1}\left(-\frac{dp}{dx}\right)^{1/n}(x)$$
$$\begin{cases} (1-y_0(x))^{1/n+1}, & 0 \leqslant y \leqslant y_0 \\ [(1-y_0(x))^{1/n+1} - (y-y_0(x))^{1/n+1}], & y_0 \leqslant y \leqslant 1 \end{cases} \quad (54)$$

where the slip velocity and the yield point are given by

$$u_w = A_1\left(-\frac{dp}{dx}\right) \quad (55)$$

and

$$y_0 = \frac{Bn}{(-dp/dx)(x)} \quad (56)$$

The slip and Bingham numbers are respectively defined by

$$A_1 \equiv \frac{akV_0^{n-1}}{H^n} \quad (57)$$

and

$$Bn \equiv \frac{\tau_0 H^n}{kV_0^n} \quad (58)$$

It turns out that the dimensionless pressure-gradient is a solution of the following equation:

$$\frac{2n+1}{n}\left(-\frac{dp}{dx}\right)^2\left[\frac{1}{\rho(p)} - u_w\right] = \left[\left(-\frac{dp}{dx}\right) - Bn\right]^{1/n+1}$$
$$\left[\left(-\frac{dp}{dx}\right) + \frac{n}{n+1}Bn\right]. \quad (59)$$

Fig. 22. Velocity contours in Bingham flow with pressure-dependent slip for $Bn = 1$ and various compressibility numbers; $A_1 = 0.1$, $A_2 = 0.01$ (exponential model), and $L = 10$.

In the case of a power-law fluid, Eq. (59) is simplified as follows:

$$\frac{2n+1}{n}\left[\frac{1}{\rho(p)} - A_1\left(-\frac{dp}{dx}\right)\right] = \left(-\frac{dp}{dx}\right)^{1/n} \tag{60}$$

In the case of a Bingham-plastic, Eq. (68) is reduced to

$$2(1+3A_1)\left(-\frac{dp}{dx}\right)^3 - 3\left(Bn + \frac{2}{\rho(p)}\right)\left(-\frac{dp}{dx}\right)^2 + Bn^3 = 0, \tag{61}$$

which has the following solution:

$$\left(-\frac{dp}{dx}\right) = \frac{1}{1+3A_1}\left(\frac{Bn}{2} + \frac{1}{\rho(p)}\right)$$
$$\left[1 + 2\cos\left[\frac{1}{3}\cos^{-1}\left\{1 - \frac{2(1+3A_1)^2 Bn^3}{(Bn + (2/\rho(p)))^3}\right\}\right]\right] \tag{62}$$

References

[1] M.M. Denn, Extrusion instabilities and wall slip, Ann. Rev. Fluid Mech. 33 (2001) 265–287.

[2] S.G. Hatzikiriakos, Wall slip of molten polymers, Progr. Polym. Sci. 37 (2012) 624–643.

[3] C. Neto, D.R. Evans, E. Bonaccurso, H.J. Butt, V.S.J. Craig, Boundary slip in Newtonian liquids: a review of experimental studies, Rep. Prog. Phys. 68 (2005) 2859–2897.

[4] T. Sochi, Slip at fluid–solid interface, Polym. Rev. 51 (2011) 309–340.

[5] C.L.M.H. Navier, Sur les lois du mouvement des fluides, Mem. Acad. Roy. Sci. Inst. Fr. 6 (1827) 389–440.

[6] D.A. Hill, T. Hasegawa, M.M. Denn, On the apparent relation between the adhesive failure and melt fracture, J. Rheol. 34 (1990) 891–918.

[7] S.G. Hatzikiriakos, J.M. Dealy, Wall slip of molten high density polyethylenes. II. Capillary rheometer studies, J. Rheol. 36 (1992) 703–741.

[8] D.S. Kalika, M.M. Denn, Wall slip and extrudate distortion in linear low-density polyethylene, J. Rheol. 31 (1987) 815–834.

[9] S.G. Hatzikiriakos, J.M. Dealy, Wall slip of molten high density polyethylene. I. Sliding plate rheometer studies, J. Rheol. 35 (1991) 497–523.

[10] J.M. Piau, N. El Kissi, Measurement and modelling of friction in polymer melts during macroscopic slip at the wall, J. Non-Newtonian Fluid Mech. 54 (1994) 121–142.

[11] M.J. Adams, I. Aydin, B.J. Briscoe, S.K. Sinha, A finite element analysis of the squeeze flow of an elasto-viscoplastic paste material, J. Non-Newtonian Fluid Mech. 71 (1997) 41–57.

[12] P. Ballesta, G. Petekidis, L. Isa, W.C.K. Poon, R. Besseling, Wall slip and flow of concentrated hard-sphere colloidal suspensions, J. Rheol. 56 (2012) 1005-1037.

[13] U. Yilmazer, D.M. Kalyon, Slip effects in capillary and parallel disk torsional flows of highly filled suspensions, J. Rheol. 33 (1989) 1197–1212.

[14] P. Estellé, C. Lanos, Squeeze flow of Bingham fluids under slip with friction boundary condition, Rheol. Acta 46 (2007) 397–404.

[15] G.V. Vinogradov, L.I. Ivanova, Wall slippage and elastic turbulence of polymers in the rubbery state, Rheol. Acta 7 (1968) 243–254.

[16] T.J. Person, M.M. Denn, The effect of die materials and pressure-dependent slip on the extrusion of linear low-density polyethylene, J. Rheol. 41 (1997) 249–265.

[17] H.C. Lau, W.R. Schowalter, A model of adhesive failure of viscoelastic fluids during flow, J. Rheol. 30 (1986) 193–206.

[18] H.S. Tang, D.M. Kalyon, Unsteady circular tube flow of compressible polymeric liquids subject to pressure-dependent wall slip, J. Rheol. 52 (2008) 507–525.

[19] H.A. Barnes, A review of the slip (wall depletion) of polymer solutions, emulsions and particle suspensions in viscometers: its cause, character, and cure, J. Non-Newtonian Fluid Mech. 56 (1995) 221–251.

[20] J. Engmann, C. Serrais, A.S. Burbidge, Squeeze flow theory and applications to rheometry: a review, J. Non-Newtonian Fluid Mech. 132 (2005) 1–27.

[21] T.Q. Jiang, A.C. Young, A.B. Metzner, The rheological characterization of HPG gels: measurement of slip velocities in capillary tubes, Rheol. Acta 25 (1986) 397–404.

[22] J.M. Piau, Carbopol gels: elastoviscoplastic and slippery glasses made of individual swollen sponges: meso-and macroscopic properties, constitutive equations and scaling laws, J. Non-Newtonian Fluid Mech. 144 (2007) 1–29.

[23] A. Lindner, P. Coussot, D. Bonn, Viscous fingering in a yield stress fluid, Phys. Rev. Let. 85 (2000) 314–317.

[24] S. Marze, D. Langevin, A. Saint-Jalmes, Aqueous foam slip and other regimes determined by rheometry and multiple light scattering, J. Rheol. 52 (2008) 1091–1111.

[25] H.A. Ardakani, E. Mitsoulis, S.G. Hatzikiriakos, Thixotropic flow of toothpaste through extrusion dies, J. Non-Newtonian Fluid Mech. 166 (2011) 1271–1762.

[26] G. Vinay, A. Wachs, J.-F. Agassant, Numerical simulation of weakly compressible Bingham flows: the restart of pipeline flows of waxy crude oils, J. Non-Newtonian Fluid Mech. 136 (2006) 93–105.

[27] F. Belblidia, T. Haroon, M.F. Webster, The dynamics of compressible Herschel–Bulkley fluids in die-swell flows, in: T. Boukharouda, et al., (Eds.), Damage and Fracture Mechanics: Failure Analysis of Engineering Materials and Structures, 2009, pp. 425–434.

[28] E. Taliadorou, G.C. Georgiou, I. Moulitsas, Weakly compressible Poiseuille flows of a Herschel–Bulkley fluid, J. Non-Newtonian Fluid Mech. 158 (2009) 162–169.

[29] D.M. Kalyon, P. Yaras, B. Aral, U. Yilmazer, Rheological behavior of a concentrated suspension: a solid rocket fuel stimulant, J. Rheol. 37 (1993) 35–53.

[30] E.G. Taliadorou, M. Neophytou, G.C. Georgiou, Perturbation solutions of Poiseuille flows of weakly compressible Newtonian liquids, J. Non-Newtonian Fluid Mech. 158 (2009) 162–169.

[31] A. Wachs, G. Vinay, I. Frigaard, A 1.5D numerical model for the start up of weakly compressible flow of a viscoplastic and thixotropic fluid in pipelines, J. Non-Newtonian Fluid Mech. 159 (2009) 81–94.

[32] S. Poyiadji, G.C. Georgiou, K. Kaouri, K.D. Housiadas, Perturbation solutions of weakly compressible Newtonian Poiseuille flows with Navier slip at the wall, Rheol. Acta 51 (2012) 497–510.